A&A 410, 911–916 (2003)
DOI: 10.1051/0004-6361:20031267

Astronomy & Astrophysics

The kinematics of the most oxygen-poor planetary nebula PN G 135.9+55.9

M. G. Richer[1], J. A. López[1], W. Steffen[1], G. H. Tovmassian[1], G. Stasińska[2], and J. Echevarría[3]

[1] Observatorio Astronómico Nacional, Instituto de Astronomía, UNAM, PO Box 439027, San Diego, CA 92143-9027, USA
e-mail: {jal, wsteffen, gag}@astrosen.unam.mx
[2] LUTH, Observatoire de Meudon, 5 place Jules Janssen, 92195 Meudon Cedex, France
e-mail: grazyna.stasinska@obspm.fr
[3] Instituto de Astronomía, UNAM, Apartado Postal 70-264, 04510 México, D.F. México
e-mail: jer@astroscu.unam.mx

Received 16 December 2002 / Accepted 2 August 2003

Abstract. PN G 135.9+55.9 is a compact, high excitation nebula that has been identified recently as the most oxygen-poor halo planetary nebula. Given its very peculiar characteristics and potential implications in the realms of stellar and Galactic evolution, additional data are needed to firmly establish its true nature and evolutionary history. Here we present the first long-slit, high spectral resolution observations of this object in the lines of Hα and He IIλ4686. The position-velocity data are shown to be compatible with the interpretation of PN G 135.9+55.9 being a halo planetary nebula. In both emission lines, we find the same two velocity components that characterize the kinematics as that of an expanding elliptical envelope. The kinematics is consistent with a prolate ellipsoidal model with axis ratio about 2:1, a radially decreasing emissivity distribution, a velocity distribution that is radial, and an expansion velocity of 30 km s^{-1} for the bulk of the material. To fit the observed line profiles, this model requires an asymmetric matter distribution, with the blue-shifted emission considerably stronger than the red-shifted emission. We find that the widths of the two velocity components are substantially wider than those expected due to thermal motions, but kinematic structure in the projected area covered by the slit appears to be sufficient to explain the line widths. The present data also rule out the possible presence of an accretion disk in the system that could have been responsible for a fraction of the Hα flux, further supporting the planetary nebula nature of PN G 135.9+55.9.

Key words. planetary nebulae: individual: PN G 135.9+55.9, SBS 1150+599A

1. Introduction

PN G 135.9+55.9 is a recently-discovered planetary nebula in the Galactic halo (Tovmassian et al. 2001; initially known as SBS 1150+599A). Its spectrum is quite unusual for a planetary nebula, presenting only the Balmer lines of hydrogen, He II$\lambda\lambda$4686, 5411, and very weak [O III]λ5007 (~3% of Hβ) in the 4000–7000 Å interval. A photoionization model analysis showed that such a spectrum implies a strongly density bounded and extremely oxygen-poor nebula ionized by a very hot star. Subsequent spectroscopy and imaging confirmed the weakness of the collisionally-excited metal lines, the high excitation, and the low oxygen abundance, around 1/500 of the solar value (Richer et al. 2002). These data also showed that the object is a point source in the continuum emission, but extended in emission lines, and suffers little reddening. Very puzzlingly, these data revealed the possibility that the Hα/Hβ ratio is variable. Additional imaging and spectroscopic observations by Jacoby et al. (2002) generally confirmed these results, though they found [Ne III]λ3869 and [Ne V]$\lambda\lambda$3346, 3426 lines stronger by an order of magnitude.

PN G 135.9+55.9 is such an important object because it has, by an order of magnitude, the lowest oxygen abundance known among planetary nebulae and will directly affect our understanding of several issues. Its study will have important implications for the understanding of the synthesis and mixing of chemical elements in metal-poor stars. PN G 135.9+55.9 may also have important implications for the early evolution of the Milky Way halo. Once this object is well-understood, it should also provide an important limit upon the pre-galactic helium abundance. The evolutionary history of PN G 135.9+55.9, particularly once a reliable distance becomes available, would provide a useful constraint upon the late stages of evolution for metal-poor stars, e.g., the time scale during pre-white dwarf evolution. More generally, kinematic studies of planetary nebulae are important for understanding the production of planetary nebulae from stellar populations (e.g., Stasińska & Tylenda 1994; Richer et al. 1997; Stasińska et al. 1998; Stanghellini & Renzini 2000; Gesicki & Zijlstra 2000). A better understanding of the production of planetary nebulae impacts a wide range

Send offprint requests to: M. Richer,
e-mail: richer@astrosen.unam.mx

of other processes, including stellar death rates, white dwarf birth rates, the mass of interstellar gas in galaxies without star formation, and the chemical enrichment of galaxies in helium, carbon, nitrogen, and *s*-process elements, among others. While PN G 135.9+55.9 will not be determinant for these latter studies, it will serve as a useful probe of a poorly populated region of parameter space.

Given the limited morphological information available for PN G 135.9+55.9 (Richer et al. 2002; Jacoby et al. 2002), a study of its kinematics has the more immediate use of helping to establish its nature and structure. We report the first high spectral resolution observations that we use to study the kinematics of PN G 135.9+55.9. In Sect. 2 we describe the observations we have undertaken. In Sect. 3 we present the results and their interpretation. We find that PN G 135.9+55.9 is best explained as an expanding elliptical envelope. In Sect. 4 we discuss how these results affect our understanding of PN G 135.9+55.9.

2. Observations and reductions

High spectral resolution observations of PN G 135.9+55.9 were obtained at the Observatorio Astronómico Nacional in San Pedro Mártir, Baja California, Mexico (SPM) with two different spectrometers at the f/7.9 Cassegrain focus of the 2.1 m telescope. The positions observed are shown in the lower right panel of Fig. 1.

First, PN G 135.9+55.9 was observed on 8 and 10 January 2002 and 14 May 2002 using the Manchester echelle spectrometer (MES; Meaburn et al. 1984). The MES is a long slit, echelle spectrometer that has no cross-dispersion. Instead, a narrow-band filter was used to isolate the 87th order containing the Hα nebular emission line. A 150 μm wide slit was used for the observations. Coupled with a SITe 1024×1024 CCD with 24 μm pixels binned 2×2, the resulting spectral and spatial resolutions are 0.1 Å/pix (equivalent to 11 km s^{-1} for 2.5 pix *FWHM*) and 1.″9, respectively. The spectra were calibrated to ± 1.0 km s^{-1} accuracy using exposures of a ThAr lamp taken immediately after every object exposure. For the January 2002 observations, the slit was oriented north-south and positioned at the positions 1–3 indicated in the lower right panel of Fig. 1. Four 30 min exposures were obtained, one each at slit positions 1 and 3 and two at slit position 2 (Fig. 1). For the May 2002 observations, six 30 min exposures were obtained with the slit oriented at a position angle of 75°. Four of these exposures were at slit position 5 and single exposures were obtained at slit positions 4 and 6 (Fig. 1). All of these MES spectra were bias-subtracted, then extracted to one-dimensional spectra, calibrated in wavelength, corrected to heliocentric velocities, and finally co-added for the observations of slits 2 and 5. The data were reduced using the Image Reduction and Analysis Facility (IRAF)[1].

Second, PN G 135.9+55.9 was observed on 19 January 2002 using the SPM REOSC echelle spectrometer. This is a conventional, cross-dispersed echelle spectrometer. Coupled with the same SITe CCD as the detector, the resulting spectral resolution was 0.16 Å/pix at He IIλ4686 (equivalent to a velocity resolution of 26 km s^{-1}), but substantially worse at Hα due to camera de-focus (see Table 1). The $2'' \times 13''$ slit was oriented east-west, as shown in Fig. 1. Two 30 min exposures of PN G 135.9+55.9 were obtained. The spectra were bias-subtracted, co-added, extracted to one-dimensional spectra, calibrated in wavelength, and finally corrected to heliocentric velocity.

Table 1. kinematic data for PN G 135.9+55.9.

slit [a]	$V_{\rm blue}$ [b] (km s^{-1})	$\Delta V_{\rm red}$ [c] (km s^{-1})	*FWHM* [d] (km s^{-1})	I(blue)/I(red)
1	-9.6 ± 0.5	43.9 ± 1.4	51.9 ± 1.0	3.34 ± 0.20
2	-9.7 ± 0.3	43.9 ± 1.4	52.3 ± 0.5	2.41 ± 0.05
3	-17.7 ± 1.4	42.5 ± 1.4	59.4 ± 2.0	0.66 ± 0.06
4	-16.6 ± 1.5	39.3 ± 1.4	47.6 ± 2.9	2.28 ± 0.31
5	-17.5 ± 0.2	43.8 ± 1.4	54.4 ± 0.3	2.05 ± 0.03
6	-25.7 ± 1.6	41.1 ± 1.4	59.7 ± 2.4	0.55 ± 0.06
7(Hα)	-19.2 ± 1.4	41.1 ± 2.0	72.1 ± 1.6	2.69 ± 0.35
7(4686)	-24.1 ± 3.0	43.7 ± 4.5	53.6 ± 5.3	1.90 ± 0.38

[a] All values are for the Hα line, except for slit 7 where results for both Hα and He IIλ4686 are given (see Fig. 1).
[b] This is the radial velocity of the blue-shifted component with respect to the heliocentric systemic radial velocity of -193.3 ± 1.3 km s^{-1}, the latter based upon the intensity-weighted average velocities for slits 2 and 5.
[c] This is the velocity difference between the blue- and red-shifted velocity components.
[d] This is the width (*FWHM*) of the two velocity components. Both components were constrained to have the same width.

For all of the spectra, the radial velocities and line widths were measured using a locally-implemented software package (McCall et al. 1985). This software fits the line profiles with sampled Gaussian profiles, fitting the systemic velocity, the line intensities, and the line widths automatically. In almost all of the slit positions, a single Gaussian was unable to reproduce the line profiles satisfactorily due to the profile asymmetry, so profiles composed of two Gaussian components were adopted. To determine the optimal line separation, the line profiles were fit with emission components whose separation was varied iteratively until the standard deviation of the residuals about the fitted profile reached a minimum. In no case was there any clear evidence for more than two velocity components in the line profiles. In Fig. 1, the Hα line profiles are shown with the fitted profile and residuals superposed. The two velocity components were constrained to have the same width. For slits 3 and 6, it was possible to fit the line profile acceptably with a single, broad Gaussian component, though these fits had larger residuals than the two component fits given in Table 1. Furthermore, the two component fits for slits 3 and 6 are otherwise very similar to those found at all other slit positions, which suggests that they are a reasonable interpretation of the line profiles.

The decomposition of the line profiles as the sum of two Gaussians was initially motivated by simplicity. However, we

[1] IRAF is distributed by the National Optical Astronomical Observatories, which is operated by the Associated Universities for Research in Astronomy, Inc., under contract to the National Science Foundation.

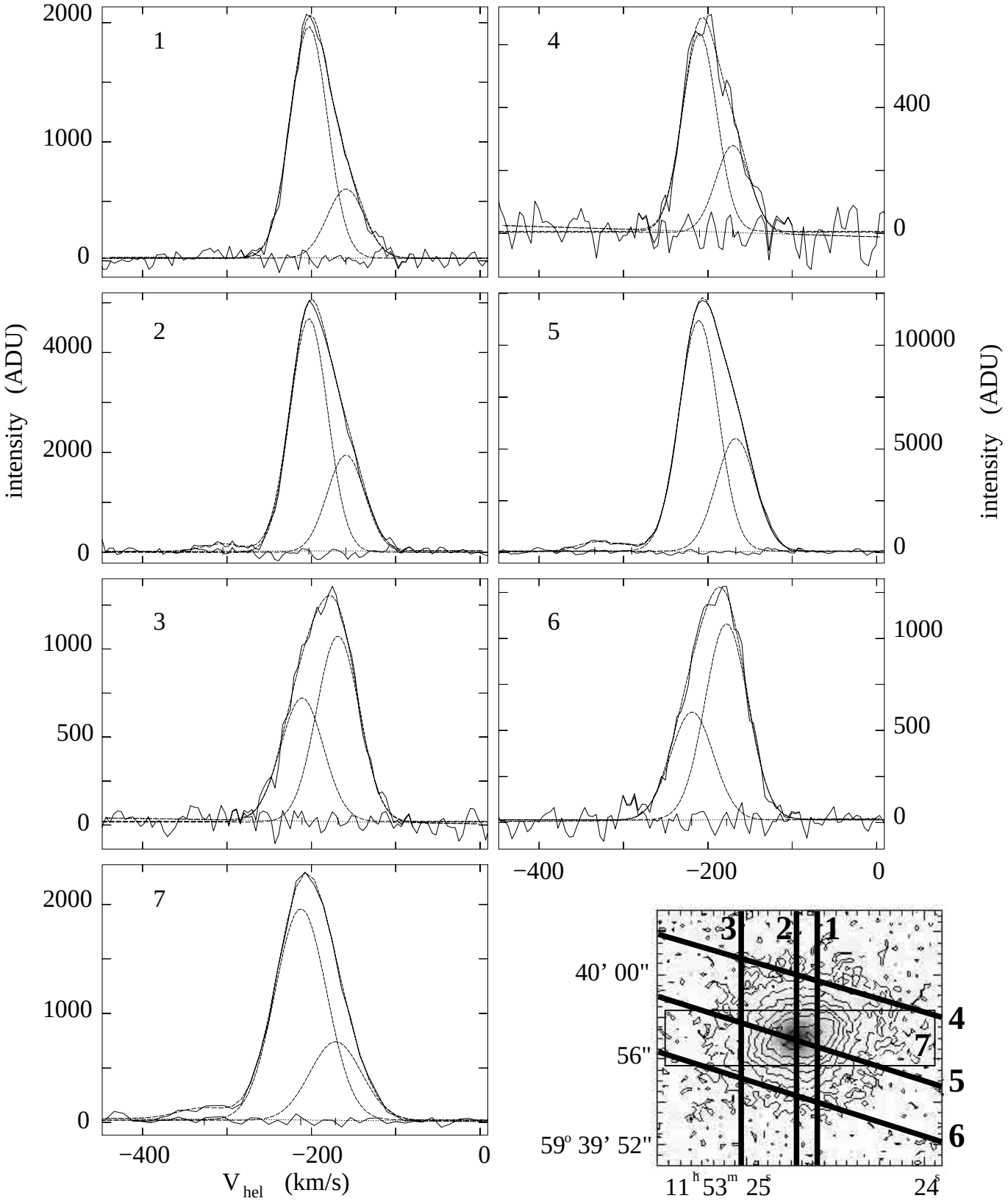

Fig. 1. This figure presents the Hα line profiles for the seven slit positions observed. The numbers in the upper left corners of each profile correspond to the slit positions shown in the lower right image (Hα contours, continuum grayscale; N is up and E to the left). The slit width for the MES observations (slits 1–6) is the same as indicated for the REOSC echelle observation (slit 7). For each profile, the fit and residuals are shown (from IRAF's splot) along with the data. The individual Gaussian components at Hα, created using IRAF's artdata.mk1dspec, are also superposed. The wavelength scale (horizontal axis) is plotted in units of the heliocentric radial velocity. The faint line visible to the blue of Hα in slits 2, 5, and 7 is He IIλ6560.

note that we can fit line profiles in different positions within the nebula where the profile shapes are different (Fig. 1) using the sum of two Gaussians and that the properties of these two components vary continuously and coherently as a function of position. For these reasons, we interpret these two components as representing the expansion of the two sides of the object. However, spectroscopy with higher resolution, both spatially and spectrally, will be required to determine whether there are indeed two distinct Gaussian components.

3. Results

In Table 1, we list the results of our line profile analyses. These results include the radial velocity of the blue velocity component, the separation of the blue and red velocity components, the width of two components, and the ratio of the intensities of the two components. The radial velocity of the blue component is given relative to the heliocentric systemic velocity of PN G 135.9+55.9. We adopted the average of the intensity-weighted mean velocities for slits 2 and 5 as the systemic velocity. The intensity-weighted mean velocities for slits 2 and 5 were computed as the average velocity of the blue- and red-shifted components, weighted according to their respective intensities. The resulting heliocentric systemic velocity for PN G 135.9+55.9 was found to be $-193.3 \pm 1.3\,\mathrm{km\,s^{-1}}$. The width of the velocity components tabulated in Col. 4 of Table 1 is the full width at half maximum (*FWHM*) of the individual velocity components (both components having been constrained to have the same width). The tabulated uncertainties are those derived from the fit to the line profiles, except in the case of the uncertainty in the line separation, which is taken to be 1.5 times the step size used to search for the minimum in the standard deviation of the fit.

As is evident from the line profiles (Fig. 1), the sequences of slit positions 1–3 and 4–6 are sequences in which the intensity of the blue velocity component decreases relative to the red component. The relative intensity of the red component increases towards the east and south. Given that these slit positions include a significant fraction of the object, the variation of the relative intensities of the blue- and red-shifted components could be more pronounced than Table 1 implies.

Likewise, the sequences of slit positions 1–3 and 4–6 are sequences in which the velocity of the blue component, V_{blue}, also increases in the last position. The largest velocities of approach of the blue component are found for slits 3 and 6, in the east and south-east, respectively.

From Table 1, it is clear that the separation of the two velocity components is approximately constant at 39–$44\,\mathrm{km\,s^{-1}}$. It is also noteworthy that the separation of the velocity components is the same in Hα and He IIλ4686. The entire nebular envelope is therefore characterized by an average apparent expansion velocity of 20–$22\,\mathrm{km\,s^{-1}}$.

Finally, we note that the widths of the two velocity components at all of the slit positions are substantially wider than those expected for a plasma at the expected temperature of 30 000 K (Richer et al. 2002). At this temperature, the line widths are expected to be $37\,\mathrm{km\,s^{-1}}$ and $19\,\mathrm{km\,s^{-1}}$ at Hα and He IIλ4686, respectively (Eq. (2-243) from Lang 1986). Instead, line widths of approximately $55\,\mathrm{km\,s^{-1}}$ are found. (We ignore the Hα line width in slit 7 due to the spectrometer defocussing.) The large observed width of the lines could arise from several causes. Given that the slit width covers a large fraction of the object, it is likely that it includes considerable kinematic structure, which would broaden the lines.

4. Discussion

Here, we develop a spatiokinematic model that explains the kinematics observed in PN G 135.9+55.9. Given the relatively low spatial resolution of both our high-resolution spectroscopy and extant imaging (Richer et al. 2002; Jacoby et al. 2002), our model will certainly not be definitive, but it should be sufficient to establish the large-scale features. A definitive model will have to await the availability of high-resolution imaging.

We have used the modeling code SHAPE (Steffen et al. 1996) to investigate the basic structure of PN G 135.9+55.9. SHAPE produces long slit spectra from a simple mathematical model of the emissivity and velocity field of three dimensional objects. These can be constructed as an arbitrary combination of individual model structures. The objects are placed at any orientation in a cubic volume, which is divided into elementary cells of uniform emissivity. The image and spectrum is calculated for each object and combined with the results of the others, taking obscuration into account, if necessary. The emission is integrated along different lines of sight in order to produce an image. The long slit spectra are produced by selecting those cells that are situated along the lines of sight covered by the slit. The emission is then mapped in position along the slit and in velocity. The result is then convolved in space and velocity according to the corresponding angular and spectral resolution. Thermal broadening is approximated by decreasing the velocity resolution appropriately. One-dimensional line profiles may then be obtained by integrating the position-velocity maps along the spatial direction. As an example application of SHAPE, see López et al. (1997).

Given the modest spatial resolution of the current observations, very detailed structural models are not warranted. However, available imaging, particularly that of Jacoby et al. (2002), indicates that the structure is not spherically symmetric, but rather elliptical. We calculated spectra for three different structures of increasing complexity. First, we constructed a spherically-symmetric model with isotropic (radial) Gaussian emissivity and velocity field that is radial and uniform (Model 1). Second, as a generalization of the isotropic model, we constructed a prolate elliptical model ("cigar"-shaped), with a Gaussian emissivity distribution, where the *FWHM* towards the poles is roughly twice as long as that in the equatorial plane (Model 2). The velocity in Model 2 is still radial, but its value in each direction is proportional to the *FWHM* of the emissivity distribution. Additionally, the brightness of one side of this model can be reduced arbitrarily compared to the other. Finally, we have considered a slow or static, isotropic, faint halo combined with Model 2 (Model 3), which seems to be distinguished from the elongated structure in the image by Jacoby et al. (2002).

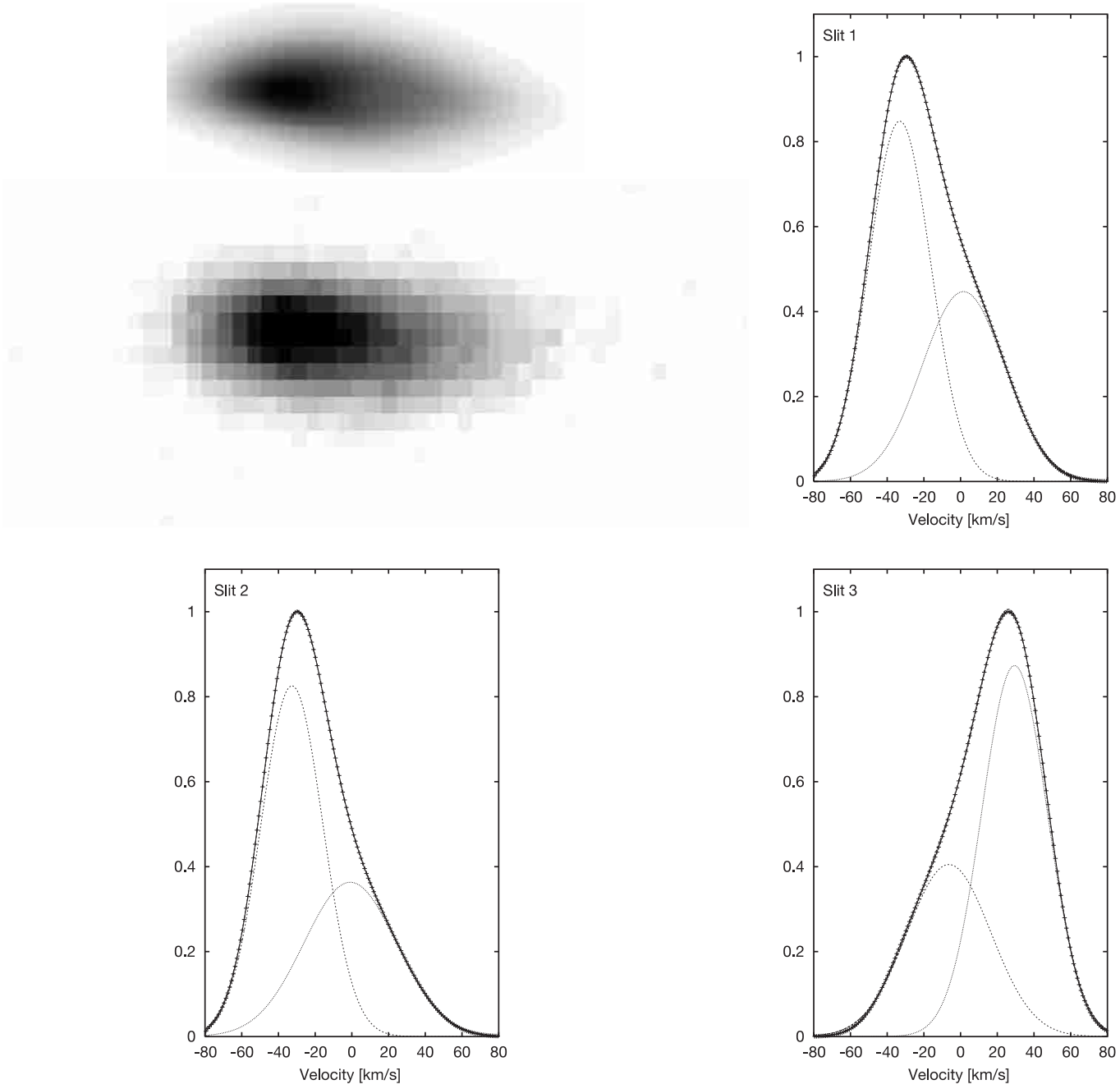

Fig. 2. Here, we present the results of the prolate elliptical model (Model 2; see text). The upper left panel presents the model position-velocity diagram for slit 2 while the middle left panel presents the observed position-velocity diagram. At bottom left is the integrated line profile for slit 2 predicted by Model 2. In the right hand panels, the integrated line profiles for slit 1 and slit 3 are presented in the top and bottom panels, respectively. These line profiles may be compared with those observed in Fig. 1. The individual profiles of the blue- and red-shifted material are also shown. The velocities are all relative to the systemic velocity.

We have evaluated slit positions 1, 2 and 3 (see Fig. 1). The best results were found for the prolate elliptical Model 2 with the following parameters: *FWHM* of volume emissivity in (x, y, z) is (3.7, 3.7, 7.5) arcsec, velocity field is radial with (V_x, V_y, V_z) of (30, 30, 70) km s^{-1} on the axes, with the position angle of z-axis at 290 degrees in the plane of the sky and inclined with respect to the line of sight by 65 degrees. In the model presented in Fig. 2, the red-shifted emission has only 20% of the intensity of the blue-shifted emission. These parameters should be considered indicative only, as a more extensive search of parameter space would likely uncover additional models that fit the data within the uncertainties. An isotropic emissivity distribution (Model 1) does not fit the data. The addition of an isotropic, faint halo (Model 3) does not significantly improve upon the agreement found between observations and Model 2. Particularly in the case of slit 2, the agreement between observations and Model 2 is excellent.

We therefore adopt 30 km s^{-1} as the expansion velocity for the bulk of the matter in PN G 135.9+55.9. Note that this is significantly different from the apparent expansion velocity

determined by fitting two Gaussians to the line profile (Sect. 2), since the fit from Model 2 takes into account projection effects.

Our modelling experiments clearly indicate that the matter distribution is asymmetric. In Fig. 2, we present the integrated line profiles for slit positions 1–3 from Model 2. In this figure, we also compare the position-velocity diagrams observed and predicted by Model 2 for slit position 2. For Model 2, we found consistency with the data only using asymmetric structures, with the red-shifted emission considerably weaker than the blue-shifted emission, reflecting the intensity ratios given in Table 1. The most plausible physical mechanisms for this emissivity asymmetry are internal reddening and an asymmetric matter distribution. Since the reddening of both the nebula and central star are low (Tovmassian et al. 2003), internal reddening does not appear to be a viable explanation for the asymmetry of the emission. It is therefore likely that the matter distribution is asymmetric and that the red-shifted emission is intrinsically weaker than the blue-shifted emission. It is also likely that high-resolution imaging will find a more complex matter distribution than the simple one adopted in Model 2, something that could be easily incorporated in future work. Indeed, even at the resolution of the Hα image presented by Jacoby et al. (2002), PN G 135.9+55.9 shows substructure.

It is clear from the preceding modelling experiments that kinematic structure within the projected area of the slit significantly affects the interpretation of the line profiles. This kinematic structure appears to account for the breadth of the two components we measure from the profiles. The large range of velocities included by the slit broadens the line profiles well beyond the thermal widths.

There are relatively few halo planetary nebulae known, and the kinematics of only a fraction of these have been studied. With the exception of NGC 4361, halo planetary nebulae appear to have expansion velocities in the 10–30 km s^{-1} range (H4-1 and BB1: Sabbadin et al. 1986; IC 4997: Miranda et al. 1996; PN G009.8-07.5: Jacoby et al. 1998). NGC 4361 has a more complex, bi-polar kinematics (Vázquez et al. 1999). Compared to other halo planetary nebulae, the kinematics we find for PN G 135.9+55.9 does not appear to be particularly atypical.

Considering the similar kinematics and line widths in both Hα and He IIλ4686, it is evident that both H^+ and He^{2+} should occupy very similar nebular volumes. This result agrees with the null detections of He Iλ5876 in low resolution spectra and confirms that the nebular envelope is very optically thin (Richer et al. 2002; Jacoby et al. 2002). The same mechanism should then be responsible for the similar line widths of both Hα and He IIλ4686.

One of the goals of the deep spectrum obtained at slit position 5 was to investigate the possible existence of broad Hα emission, >few $\times$ 100 km s^{-1}. No such broad component was found, in agreement with the results of Tovmassian et al. (2001). This result rules out the possibility that PN G 135.9+55.9 contains an accretion disk that emits a significant fraction of the Hα flux, even for the case of a face-on disk (e.g., Horne & Marsh 1986). Consequently, we can discard the possibility that PN G 135.9+55.9 contains a close interacting binary with an accretion disk that could introduce a distinct Hβ/Hα ratio or any sort of variability.

To summarize, the kinematics of PN G 135.9+55.9 allow us to impose important constraints upon the structure of this most oxygen-poor planetary nebula. Globally, the kinematics can be interpreted as an expanding elliptical envelope. Our modelling experiments indicate that the matter distribution is asymmetric, a prolate ellipsoid fitting best, with the blue-shifted emission several times stronger than the red-shifted emission. The apparent line widths we find are substantially larger than the thermal widths, though this appears to be due to the kinematic structure projected within the area of the slit. There is no indication of the presence of an accretion disk or a binary companion. Finally, given the extreme nature of its spectrum, that the kinematics of PN G 135.9+55.9 are similar to those of other halo planetary nebulae is additional evidence in favour of it in fact being a planetary nebula.

Acknowledgements. MGR, JAL, and GT thank G. García, G. Melgoza, S. Monrroy, and H. Riesgo for their able assistance with the observations at SPM. We gratefully acknowledge financial support from CONACyT projects 32214-3 (JAL), 34521-E (GT), and 37214-E (MGR, GS) and DGAPA projects IN100799 (MGR), IN114199 (JAL), and IN118999 (JE, GT).

References

Gesicki, K., & Zijlstra, A. A. 2000, A&A, 358, 1058
Horne, K., & Marsh, T. R. 1986, MNRAS, 218, 761
Jacoby, G. H., Feldmeier, J., Claver, C. F., et al. 2002, AJ, 124, 3340
Jacoby, G. H., de Marco, O., & Sawyer, D. G. 1998, AJ, 116, 1367
Lang, K. R. 1986, Astrophysical Formulae (New York: Springer-Verlag)
López, J. A., Steffen, W., & Meaburn, J. 1997, ApJ, 485, 697
McCall, M. L., Rybski, P. M., & Shields, G. A. 1985, ApJS, 57, 1
Meaburn, J., Blundell, B., Carling, R., et al. 1984, MNRAS, 210, 463
Miranda, L. F., Torrelles, J. M., & Eiroa, C. 1996, ApJ, 461, 111
Richer, M. G., McCall, M. L., & Arimoto, N. 1997, A&AS, 122, 215
Richer, M. G., Tovmassian, G., Stasińska, G., et al. 2002, A&A, 395, 929
Sabbadin, F., Strafella, F., & Bianchini, A. 1986, A&AS, 65, 259
Stanghellini, L., & Renzini, A. 2000, ApJ, 542, 308
Stasińska, G., Richer, M. G., & McCall, M. L. 1998, A&A, 336, 667
Stasińska, G., & Tylenda, R. 1994, A&A, 289, 225
Steffen, W., Holloway, A. J., & Pedlar, A. 1996, MNRAS, 282, 1203
Tovmassian, G. H., Stasińska, G., Chavushyan, V. H., et al. 2001, A&A, 370, 456
Tovmassian, G. H., Stasińska, G., Napiwotski, R., Richer, M. G., & Fullerton, A. W. 2003, in preparation
Vázquez, R., López, J. A., Miranda, L. F., Torrelles, J. M., & Meaburn, J. 1999, MNRAS, 308, 939